MetaBioLiq: A Wearable Passive Metasurface Aided mmWave Sensing Platform for BioFluids

Baicheng Chen
University of California San Diego
La Jolla, CA, USA
b3chen@ucsd.edu

John Nolan
University of California San Diego
La Jolla, CA, USA
jmnolan@ucsd.edu

Xinyu Zhang
University of California San Diego
La Jolla, CA, USA
xyzhang@ucsd.edu

ABSTRACT

Human external biofluid (e.g., sweat, urine) contains vast health data that is readily harvestable. Currently, wearable sweat sensors require an electrochemical-based approach that is used in single use, creating environmental pollution as people track their exercise in the wild. Moreover, such solution relies on a battery-powered design, which brings battery health and thermal related issues. We present MetaBioLiq, a 3D printed wireless-readable sweat sensing system that offers continuous monitoring, featuring completely passive, environmentally friendly, and easily accessible. MetaBioLiq is developed upon sweat liquid's resonance upon high frequency RF interaction, with different sweat content driving RF resonance characteristics. To activate such resonance, we design 3D PolyLactic Acid (PLA) structures that capture e-field energy from the air, and tunneling it to the sweat. Once the resonance effect occurs, we analyze return signal from a wireless RF receiver to decouple the sweat's resonance. Lastly, we evaluate MetaBioLiq's performance with 24 artificial sweat samples containing different levels of glucose, electrolytes, and fat. MetaBioLiq proves its effectiveness with 95% liquid level detection performance, and 96% sweat liquid identification performance. We further investigate MetaBioLiq's robustness and reliability, as well as limitations. Overall, MetaBioLiq shows promising results to expand the realm of mobile continuous sensing to microscopic realm untangible in the past.

CCS CONCEPTS

• **Computer systems organization → Embedded and cyber-physical systems**.

ACM MobiCom '24, November 18–22, 2024, Washington D.C., DC, USA

ACM ISBN 979-8-4007-0489-5/24/11
https://doi.org/10.1145/3636534.3690687

KEYWORDS

Metasurface, mmWave Sensing, 3D Printing, IoT

ACM Reference Format:
Baicheng Chen, John Nolan, and Xinyu Zhang. 2024. MetaBioLiq: A Wearable Passive Metasurface Aided mmWave Sensing Platform for BioFluids. In *The 30th Annual International Conference on Mobile Computing and Networking (ACM MobiCom '24), November 18–22, 2024, Washington D.C., DC, USA.* ACM, New York, NY, USA, 15 pages. https://doi.org/10.1145/3636534.3690687

1 INTRODUCTION

Human sweat has been extensively studied as a noninvasive biomarker[33], health indicator, and forensic evidence [59] for a long history. Past research has shown that even a slight level of dehydration can introduce cardiorespiratory stress, compromise thermoregulation, and significantly alter physical / cognitive performance, further initiating a cascade of physiological changes [5]. With increasing efforts in sweat sensor technologies, the wearable sweat sensor market is projected to reach 3 billion USD by 2030 [42]. Existing sweat/biofluid sensing platforms depend on electrochemical [5] or chemochromic (visual) patches [64] for measurements and an external wireless module for communication. Such techniques require patch/battery replacement, which fails continuous monitoring, restricts user mobility, and increases cost [5]. With such limitations, analytic applications, such as continuous sleep/athletic monitoring, are hampered.

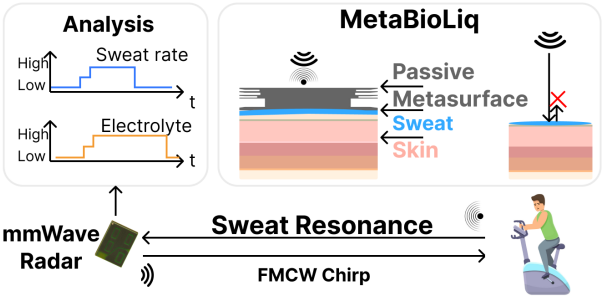

Figure 1: MetaBioLiq, a wearable 3D-printed metasurface aided mmWave sensing platform, that unlocks human biofluid information with microliters of sample fluid such as human sweat.

Microliters of sweat fluid have an insignificant presence in radar reflection at a remote distance. Existing wearable sweat sensors are based on electrochemical properties for quantity and content analysis [24]. They face two main challenges in usability, i) periodic electrode replacement / patch and ii) power supply for electrode readings, processing, and wireless communication. Upon contact, either chemo-sensistive material alters electrical resistance or electrodes sense liquid impedance upon the presence of various sweat content at different levels (e.g. water, electrolyte, fat, etc.). However, such a technique requires a liquid flow design that fixes the channel quantity, replaces the complete electrode patch upon single use, and attaches wireless communication in mobile use cases, making the power supply an inevitable challenge. On the other hand, chemochromic sensors [64] are often made into single-use camera-ready patches that change visible color upon contact with different concentrations of a certain sweat substance (e.g., electrolyte for pH strip). Such a technique makes continuous measurement nearly impossible. Given the importance of sweat analytics to healthcare, it is of key interest for future healthcare system to come up with a well-rounded solution that eliminates usability issues.

To this end, we present MetaBioLiq, a fully passive, continuous, and wearable biofluid sensing system based on a 3D printed metasurface. The overall idea is illustrated in Fig. 1. Lacking radar reflection strength, we apply a wearable metasurface to amplify the reflection signal from microliters of sweat fluid. By altering a block of PolyLactic Acid (PLA) material's 3D printing parameters and geometric shape, it can serve as a mmWave microscope at remote distance that resonates with a thin layer of liquid in contact. With a skin-fitting metasurface design that resonates with the liquid content inside the designed cavity, the metasurface can tell how much sweat is present, as well as the content of the liquid. Given the mmWave radar's ability to accurately localize the metasurface and continuous extract sweat's spectrum pattern, we can now monitor a person's sweat continuously over a long period of time and advise interventions accordingly.

To achieve MetaBioLiq, we must first solve the following challenges: *(1) Sweat Radar Cross Section (RCS).* Human sweat on the skin is only millimeter thick. Compared to skin reflection, its mere presence is hardly identifiable. To sufficiently distinguish sweat reflection from surrounding reflection, we utilize a sweat impedance-matched metasurface at a mmWave frequency that is sufficiently tall to make the whole structure easily distinguishable. Using a mmWave radar that sends FMCW chirps as remote query device, we ensure that the structure's height sufficiently stands out versus the surrounding, resulting in a fully passive sweat sensor tag that resonates with sweat liquid. *(2) Sweat Signal to Interference/Noise Ratio (SINR).* From a unit volume of sweat per skin surface area over a given time measurement, only microliters of sweat can be collected from a square inch of skin in one hour, assuming that the average number of sweat glands under the skin functions normally [73]. This tiny volume has resulted in commercial-off-the-shelf (COTS) wireless sweat sensor solutions to set an enormous startup time until the sweat reservoir is completely full (e.g., 45 minutes [48]). In addition, sweat must be isolated from the skin to decouple any interference. Not to mention that sweat is 99% water and only 1% remaining substance, with salt and fat being the dominant elements [43]. To improve the SINR in sensing microliters of sweat, we optimize our metasurface to resonate with a tiny amount of sweat inside an open cavity with maximum focus on the sweat layer only, and minimize the impact of skin layer. We then explore sweat content variation impact to radar reflection pattern based on different solute's impact on dielectric parameter change, resulting in frequency domain features under radar inspection. *(3) Radar Handicap.* COTS mmWave radar as a emerging sensing modality offers high frequency and multi-GHz bandwidth to encapsulate sweat resonance with higher dynamic range. However, COTS Frequency Modulated Continuous Wave (FMCW) mmWave radar's amplitude reading is integral throughout its bandwidth, making the sweat query result more complicated than our desired output. To recover mmWave band frequency domain information, we model the end-to-end RF signal-to-sweat interaction following the Cole-Cole model [35], and design a calibration scheme that brings the ADC sampled data one step closer to the mmWave band spectrum. We then verify that the calibration result would match the simulated result. *(4) User Dependence.* Each person's habit is different, given an open cavity design, different users wearing the same metasurface can experience frequency drift due to skin occupying some of the liquid cavity space. Thus, we design a one-time soft calibration procedure that enrolls each user's unique pattern to better bring recovered mmWave spectrum closer to model result.

After solving these problems, we prototype the sweat sensor metasurface in the form factor similar to a COTS smart watch (L×W×H: 40×40×27 mm). A single sensor costs around $1, and takes around 3 hours to 3D print. We have conducted experiments in real-world setup where the sensor is placed on human subjects. We utilize artificial sweat that mimics human sweat content's saline, glucose, and lipid concentration [46, 47, 62]. MetaBioLiq's end-to-end system achieves 95% accuracy in sweat rate detection and 96% accuracy in sweat content classification performance. In addition, the performance of MetaBioLiq is maintained above 90% in various stress tests where the distance and angle vary to 1.5m and ±28°, respectively.

To this end, we present the following contributions in this work:

System	Sensing Modality/BW	Volume	Capability	Distance	Remote Setup
LiqRay [57]	RF/900Mhz	$\geq$ 100mL	8 Liquid	$\leq$ 1m	✓
TagScan [66]	RFID/4MHz	$\sim$ 100mL	10 Liquid	4.5m	✓
WiMi [22]	WiFi CSI/20MHz	$\sim$ 1800mL	10 Liquid	3 m	✓
Vi-Liquid [29]	Vibration/1.6kHz	$\sim$ 250mL	30 Liquid	Contact	Contact
LiquID [18]	UWB/1GHz	$\sim$ 2736mL	33 Liquid	$\leq$ 1m	✓
Akte-LiquID [61]	Ultrasound/6kHz	100mL	20 Liquid	$\leq$ 15cm	Short range
FG-LiquID [40]	mmWave/2.16GHz	350mL	30 Liquid	2 m	✓
LiqDetector [67]	mmWave/4Ghz	$\geq$ 200mL	6 Liquid	50 cm	✓
BioScatter [32]	WiFi + Electrode/$\sim$	15mL	Artificial Sweat	2 m	Patch
Wired Resonator [15]	VNA/12Mhz	10mL	Artificial Sweat	Contact	Waveguide + Resonator
MetaBioLiq	**mmWave/5.5GHz**	**0.67 mL**	**Artificial Sweat**	**1.5 m**	**Radar + Metasurface**

Table 1: MetaBioLiq compared with existing liquid sensing and sweat sensing work

- We design a continuous wireless sweat monitoring system via fully passive mmWave metasurface capable of characterizing milliliters of sweat.
- We design and fabricate the metasurface using 3D printed PLA material on COTS 3D printers.
- We turn mmWave radar into a pseudo vector network analyzer to infer sweat frequency response remotely.
- We develop corresponding signal processing and decision algorithm for sweat content extraction.
- We conduct extensive evaluation on feasibility, usability, and robustness of the sweat sensing system.

2 RELATED WORKS

2.1 Wireless Liquid/Sweat Sensing

Existing wireless liquid and sweating sensing literature can be categorized into two classes, i) radio path loss-based [18, 22, 57, 66] and ii) electrode sensor with wireless communication module [11, 32]. acoustic[61], tactile[29], resonator[15] modals are often contact-based or short in range. Certain reflection-based sensing modalities also use mmWave signals [40, 67, 69], but they are constrained by a large volume of liquid body (i.e., hundreds of milliliters), which is nowhere close to the realistic volume of human sweat. Some even require the addition of a bulky Fresnel lens mounted on the radar to focus RF energy in a very constrained scenario [28]. Using such systems in sweat sensing, the signal from the presence of a liquid and its liquid content is heavily buried with background noise from the human arm or body, making it inseparable for deterministic conclusions. As shown in Table 1, all existing systems focus on large volumes of liquid that are impractical for sweat quantity, and most of them are far from revealing subtle differences in liquid content. MetaBioLiq is the first wireless liquid/sweating sensing work that pushes wireless liquid sensing to the microliter level using a mmWave metasurface.

2.2 Wireless Health Monitoring

During the past decade, wireless health monitoring application have been widely explored. From macromotion for elder fall detection [65], human activity recognition [72], vital sign monitoring [26], to emotion recognition [76], and disease prediction [75]. Motion and acoustic channels have enabled many wireless health monitoring use cases. To date, MetaBioLiq is the first paper to exploit completely passive wireless biofluid sensing using a mmWave metasurface.

2.3 3D Printed Biosensors

With increasing accessibility of the COTS 3D printer, it is now widely used to rapidly prototype dielectric metasurfaces [51] and even biocompatible sensors. Commonly, 3D printed devices in health applications serve as adapters/stent/support devices in wearable [34], earable [17], or rehab [74] settings. The growing development of 3D printers has nurtured new capabilities of 3D printed devices to replace pressure, stress, and tactile sensors in biomedical applications [1, 58]. Some work also designed casings to better facilitate sweat electrodes [37]. MetaBioLiq is the first work to achieve a completely passive wireless sweat biosensor using a mmWave metasurface.

3 PRELIMINARY

3.1 Sweat RF Sensing

Human sweat from the single largest organ (i.e., skin) occurs spontaneously, and involves highly dynamic physiological change [10]. In the process of sweating, a variety of nutrients are released (e.g., electrolytes, glucose, fat, hormone) along with 99 % of water that form the general definition of sweat liquid [43]. With sweat being 99% water, water property is dominant under radio frequency observation, setting a baseline for sweat content properties. When adding an electrolyte sweat concentration to a water sample, its RF

dielectric conductivity increases and its relative permittivity decreases, causing a uniquely distinguishable signature under RF interrogation [21, 23]. Similarly, glucose [41, 73] and fat molecules [77] in aqueous solution exhibit their own pattern. With different concentrations of each substance in a sweat sample, its sweat signature under RF interaction reflects its content detail, as shown in Fig. 2.

mmWave sensing technology has now shown its high frequency strength with high directionality, high bandwidth, and low latency characteristics. It has empowered diverse applications such as remote human localization, object tracking, and micromotion capture [56, 63, 68, 71]. Compared to low-frequency RF modalities such as WiFi [22], UWB[18], acoustic[40], or RFID [66], mmWave's high frequency stands out with the capability to focus on a small sweat sample and extract fine-grained information with minimal setup requirement.

However, a major challenge for remote mmWave sweat sensing is that sweat is released in tiny volumes over a long period of time (e.g., hundreds of microliters per square inch per hour) [14, 25]. Making remote sensing nearly impossible without the aid of a zooming tool. As shown in Fig. 3, liquid that is drastically different in dielectric constant shows nearly identical reflection amplitude and phase within the 60 GHz mmWave band. For the COTS device [48], 45 minutes of rigorous exercise are needed before the electrode sweat sensor receives meaningful readings.

Hypothesis: Given a wearable mmWave microscope that focuses on sweat, mmWave sensing device can remotely query the microscope and decode the biofluid information. Different sweat content creates a distinct and persistent RF signature with a sufficient SINR that distinguishes itself from a noisy background (e.g., skin). *Overall, a human subject wearing a mmWave microscope can provide continuous sweat rate and content information, based on the signature reflected from the microscope to a remote querying device.*

3.2 Viewing Sweat Under RF Microscope

We first explore the RF behavior of sweat by modeling it as a thin layer of water, as shown in Fig. 4. When the wavefront of a single-tone electromagnetic wave enters a thin layer of water from the air, several interactions occur. The air-water interface causes part of the energy to reflect; after the wave enters the water layer at certain angles, following Snell's law, water itself absorbs that energy like a capacitor, and if

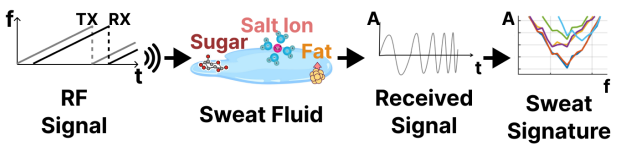

Figure 2: Modeling sweat with RF signal.

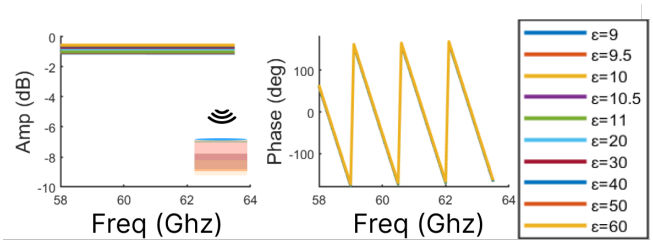

Figure 3: Reflection signal without metasurface. Both amplitude and phase doesn't show significant change despite large variation in liquid content (ϵ = 9-60).

the layer is thin enough, the remaining energy then passes through.

Based on the liquid dielectric characteristics, we can model its distinct relaxation process using Cole-Cole model [12]:

$$\hat{\epsilon}(\omega) = \epsilon_\infty + (\epsilon - \epsilon_\infty) \sum_{j=1}^{n} \frac{g_j}{[1 + (i\omega\tau_j)]}$$
$$g_j = \frac{\epsilon_j - \epsilon_{\infty j}}{\epsilon - \epsilon_\infty}; \epsilon_{\infty j} = \epsilon_{j+1}; \epsilon_1 = \epsilon; \epsilon_{\infty n} = \epsilon_\infty \quad (1)$$

where $\hat{\epsilon}(\omega)$ is the frequency dependent liquid permittivity, ω is the frequency, n is the number of separable dispersion steps j of relaxation time τ_j, dispersion amplitude $\epsilon_j - \epsilon_{\infty j}$ and weight g_j.

Which leads to a wrapped reflection model: [27, 45]:

$$Z(\omega) = \frac{1}{i\omega\epsilon_0\epsilon(\omega)D}$$
$$\Gamma(\omega) = \frac{Z(\omega) - Z_0(\omega)}{Z(\omega) + Z_0(\omega)} \quad (2)$$

where $Z(\omega)$ is the frequency dependent impedance of liquid sample, and $Z_0(\omega)$ is the RF probe's impedance.

As shown in Fig. 5, a vector network analyzer (VNA) S11 plot clearly indicates the similarity (e.g., salt solution 1 vs. salt solution 2) and difference (e.g., salt solution 1 vs. sugar solution 1) between various solutions. To summarize the model, the reflection properties of sweat liquid exhibit a pattern that is dependent on frequency, and its amplitude and phase information carry details about solutes, such as the level of salinity, glucose level and fat content.

3.3 Proof-of-Concept

To validate the above Cole-Cole model, we 3D print a liquid cavity that holds liquid to be examined under a mmWave VNA [3]. The VNA sends planar waves to the surface of the liquid and records S11 reflection over a 10 GHz bandwidth centered at 60 GHz mmWave band. As shown in Fig. 5, both amplitude and phase patterns are analyzed for inter- and intra-group analysis. With air representing empty cavity baseline, salt solution vs glucose solution's pattern is

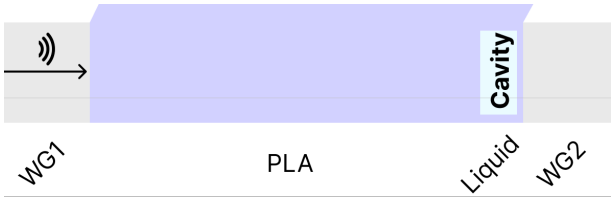

Figure 4: Cole-Cole model with 3D printed PLA block holding liquid under VNA inspection. Two waveguide(WG) seal the PLA block to measure accurately.

uniquely distinguishable across multiple mini frequency bands. In addition, such signature is consistent across reading with salt solution 1 vs. salt solution 2 being nearly identical, and the same applies to glucose solution intra-group comparison. In summary, under mmWave inspection, both amplitude and phase characteristics are deterministic, unique, and persistent for each type of aqueous solution under close observation.

4 METABIOLIQ SYSTEM OVERVIEW

We describe the major components that achieve a 3D printed metasurface aided mmWave sensing platform for biofluid sensing; the flow chart of the system is shown in Fig. 6.

Turning radar into network analyzer: MetaBioLiq adopts a miniaturized mmWave radar that is smartphone integratable to query sweat's content. After receiving the ADC samples from the radar baseband, we perform signal processing techniques such as noise reduction, signal boosting, and baseband-RF mapping via an adaptive calibration scheme. The calibrated signal in the frequency domain then undergoes a feature extraction and classification algorithm to infer the liquid level inside the cavity, as well as sweat content.

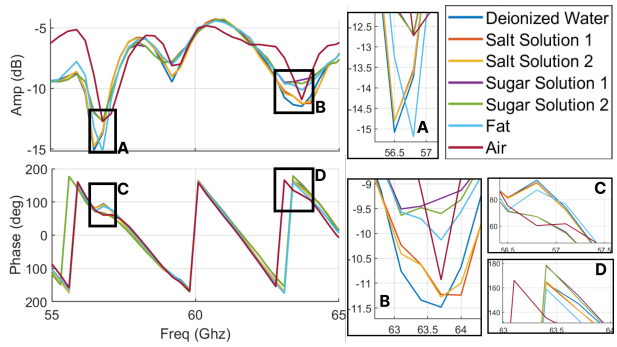

Figure 5: VNA measurement of different liquid under behind PLA block shown in Fig. 4. Both the magnitude and phase components show significant difference at multiple regions of interest. Box A and B are from amplitude plot, box C and D are from phase plot.

Metasurface design and fabrication: Given sweat's fluid nature, we design a liquid cavity with PLA material's hydrophic [20] surface to contact sweat directly under the metasurface. To better work with our mmWave radar, we first optimize the 3D geometry of the metasurface to shift the frequency of interest to the radar bandwidth. Then, we fine-tune the metasurface to focus on changes in the sweat layer, and become immune to the skin layer.

5 METASURFACE DESIGN

5.1 Dielectric Modeling

The MetaBioLiq metasurface consists of multiple layers of PLA material with variable filling factor. Compared with a single block of material, multi-layer design enables flexible manipulation of frequency selective equivalent dielectric permittivity $\epsilon_x(\omega)$ calculation [53] as follows:

$$\epsilon_x(\omega) = f\epsilon_{air}(\omega) + (1-f)\epsilon_{PLA}(\omega), \tag{3}$$

where $(1-f)$ is the ratio that PLA material occupies in the modulating layer, f is the filling factor for air. Multiple layers of PLA separated by fixed design spacer form a uniform structure that matches impedance of input and output material, which is air and sweat liquid, respectively. Such variable enables efficient tuning and prototyping of the metasurface. A graphical demonstration is shown in Fig. 7.

Based on the above closed form equivalent permittivity model for a single modulating layer, we can further develop the closed form transfer matrix model for the entire metasurface structure [53] as follows:

$$M_t = \prod_{i=1}^{N} M_i^{layer} \times M_i^{spacer} \tag{4}$$

where M_i^{layer}, and M_i^{spacer} are the modulating layer matrix, and spacer matrix, respectively.

The overall matrices for the modulating layer and spacer layers[52] are calculated using:

$$M_{layer} = M_{inter}^1 M_{delay} M_{inter}^2 \tag{5}$$

$$M_{delay} = \sum_x \begin{bmatrix} e^{j\beta_0 d\sqrt{\epsilon_x}} & 0 \\ 0 & e^{-j\beta_0 d\sqrt{\epsilon_x}} \end{bmatrix}; M_{inter} = \sum_x \frac{1}{T_x}$$

where M_{inter}, M_{delay}, d, and T_x are the interface matrix, phase delay through the layer, thickness of the layer, and Fresnel coefficient, respectively. Using Fresnel coefficients and Maxwell continuity equations for each medium [60], the output model should accurately describe the overall modulation in incidental wave.

Based on this model, we develop an optimizer that outputs geometric parameters that resonate best with a given incident frequency and layer number. To verify the MetaBioLiq metasurface optimizer, we fabricate a sample model. We first test different sizes of the metasurface that relate to the radar

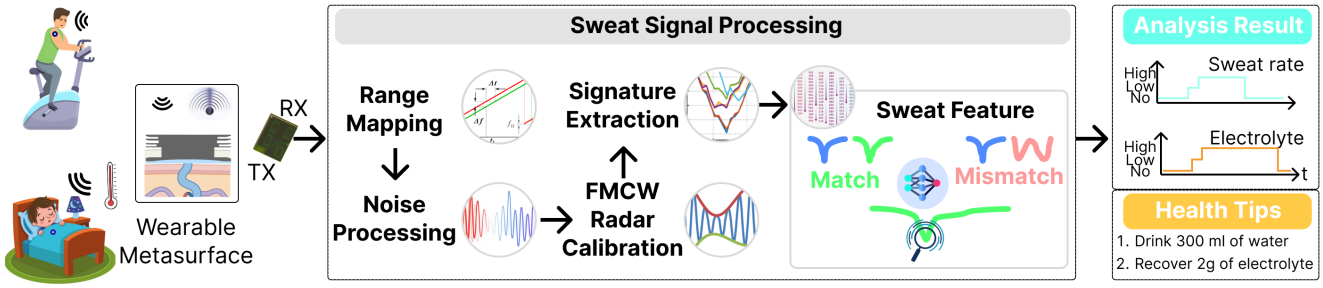

Figure 6: MetaBioLiq platform comprises 3D printed wearable metasurface, mmWave radar, sweat feature extraction, sweat content identification, and analysis feedback modules.

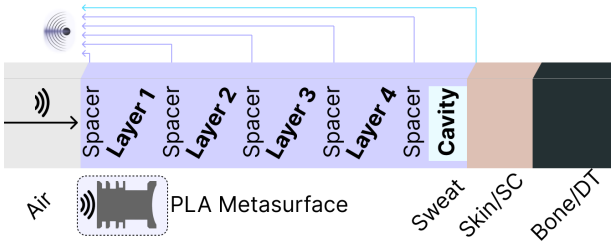

Figure 7: Transfer Matrix Model

cross section, and empirically verified a 3 x 3 cm cross section showing strong enough signal against background. More details for size determination are given in Sec. 9.3.1. Next, we utilize radar's 5.5 GHz bandwidth to calculate the physical range resolution, which is 2.7 cm. Thus, we set our metasurface's initial thickness to 2.7cm, which helps when isolating metasurface reflection against background reflection (e.g., skin/body). As shown in Fig. 8, the multilayered structure shows a better resonance effect at a given frequency compared to a single block of material It is worth mentioning that the 4-layer design ceils the resonance effect in simulated S11 reflection plot, and the geometry for each layer's PLA internal structure in shown in Fig. 8(a).

We further explore the sensitivity of the generated metasurface to the sweat content. In high frequency structural

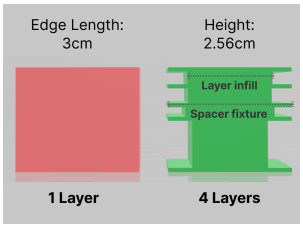

(a) Solid vs Layered design

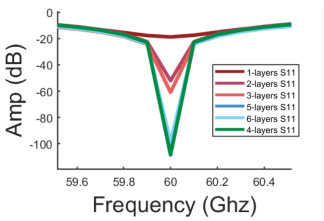

(b) 4 layer design is optimal

Figure 8: Metasurface design from a block of PLA material to layered geometric structure.

simulator (HFSS), we accurately model the geometry of optimizer generated metasurface, as well as dielectric parameters for human tissue [70]. We suppose that the metasurface is placed on the wrist like a watch, and model the skin [30] to be 3mm with the deeper tissue empirically being bone structure. Generally, sweat covers the skin surface and mmWave hardly penetrate 1mm into the skin due to the attenuation of the moisture content and permittivity delta [7]. For the sweat content, we first model it as pure water [44] with $\epsilon = 10$, and alter its dielectric constant with various order of magnitudes to simulate different levels of solute content [23]. As shown in Fig. 9, a change of $\Delta\epsilon = 0.1$ will signify noticeable frequency shift in multiple regions of interest, while a smaller $\Delta\epsilon$ is nearly identical to pure water.

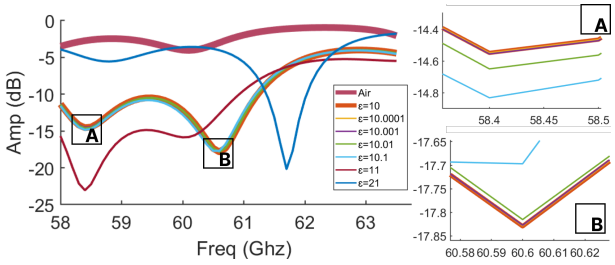

Figure 9: Metasurface sensitivity to liquid dielectric constant change. ϵ delta of (10,1,0.1,0.001,0.0001) from pure water of ~10 at 60 GHz [44] at room temperature. A delta of 0.1 is considered significant given relative ratio to pure water at two frequencies is distinguishable at frequency spot A and spot B.

5.2 Optimizing the Metasurface Structure

To this stage, the metasurface can effectively capture the dielectric change in the sweat layer; however, the dynamic nature of human skin must be taken into account. We further optimize the model to become immune to the skin layer. Based on the previous optimization model [53, 53], we can maximize sensitivity to the sweat layer and minimize the

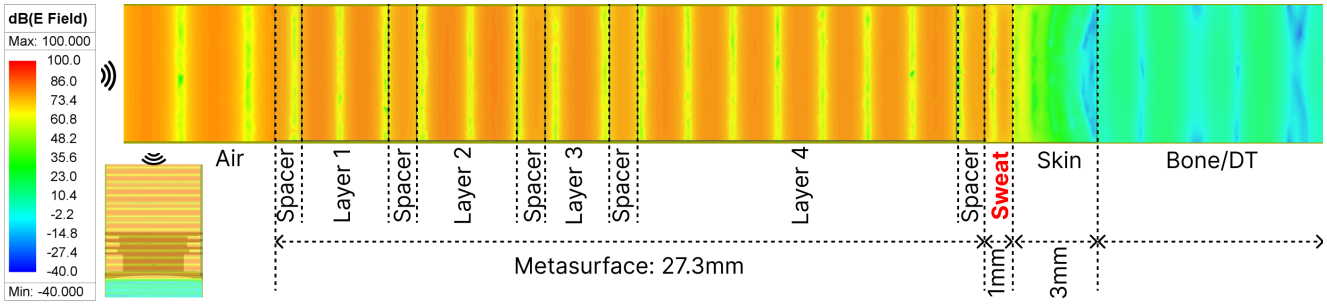

Figure 10: HFSS electric field plot heat map that represents response strength across air, metasurface, sweat, skin, and bone/deeper tissue(DT) layers. Sweat layer's response is significantly stronger than the skin, making the reflection response immune to skin's change.

sensitivity toward skin layer [60]. The optimizer calculates the cost of the design for and iterates until the cost function converges given the modulation criteria is met for each layer. The cost function is as follows:

$$cost(\omega) = \sum_{1,2} |S_{xx}(\omega)| + |S_{21}(\omega) - S_{21d}(\omega)| \tag{6}$$

where S_{xx} can be substituted with S_{11} and S_{22} as reflection S-parameters from the top and bottom port of incidence, respectively. S_{xyd}, ϕ_d are the desired propagation S-parameters, and the desired phase shift. As shown in Fig. 10, the resulting model's sweat layer response is significantly stronger than the skin layer as the signal diminishes after the sweat layer. This substantiates the effectiveness of MetaBioLiq metasurface resonating with sweat layer. This aligns with previous research findings that mmWave dosimetry on skin is minimal [7].

6 TURNING RADAR INTO NETWORK ANALYZER

At this point, the metasurface that captures and reflects sweat content in mmWave band, we apply hardware limitations of a COTS FMCW mmWave radar and decode sweat information from radar's baseband ADC sample.

6.1 Range Binning

FMCW mmWave radar compares the frequency shift of received (RX) chirps to that of transmitted (TX) chirps $x(t)$ in time domain [28]. This frequency shift is directly proportional to the time delay τ between the TX and RX signals, which is a measure of the round-trip distance $2R$.

$$\begin{aligned} x(t) &= A_0 e^{j(\omega(t)*t+\theta_0)} \\ \tau = \frac{2R}{c}; \omega(t) &= \omega_0 + \frac{B}{t_c}t \end{aligned} \tag{7}$$

where A_0 is the transmitted power amplitude, $\omega(t)$ is TX chirp's representation in frequency domain, B is the total bandwidth and θ_0 is the initial phase offset. We can then rewrite the TX chirp in the frequency domain as:

$$x(w) = A_0 e^{j(\omega(t)^2 \frac{t_c}{B} - \omega(t)\omega_0 \frac{t_c}{B} + \theta_0)} \tag{8}$$

where t_c is the chirp duration, and $\overline{x(w)}$ is the conjugate of $x(w)$. The RX side signal before mixing $y'(w)$ and after mixing $z(w)$ with conjugate of TX signal $\overline{x(w)}$ can be modeled as [28]:

$$\begin{aligned} y'(w) &= A_0 \sum_{n=0}^{\inf} a_n e^{-2n\omega C_1} e^{-j(2n\omega C_2 - \omega(t)^2 \frac{t_c}{B} + \omega(t)\omega_0 \frac{t_c}{B} + \omega\tau - \theta_0)} \\ z(w) &= A_0^2 \sum_{n=0}^{\inf} a_n e^{-2\omega C_1} e^{-j(2n\omega C_2 + \omega\tau)} \\ C_1 &= \frac{\sqrt{\epsilon_r} tan(\delta) * d}{2c}; C_2 = \frac{\sqrt{\epsilon_r} * d}{c} \end{aligned} \tag{9}$$

where d is the distance/thickness into material. n is the number of reflection occurrences within the material. Although a larger n represents more accurate modeling, the signal energy quickly approaches zero with n greater than 3. When ADC samples the mixed signal,

$$R(\tau) = \sum_{t=\tau_{RX0}}^{\tau_{RX0}+t_c} A_0 e^{-2\omega C_1} e^{-j(2n\omega C_2 + \omega\tau)} \tag{10}$$

where τ_{RX0} is time delay from TX starts chirp emission to ADC sample after . The total number of ADC sample is usually a power of 2 and higher number leads to more frequency resolution. This model also means that if the metasurface is not the first object in line of sight, its characterization will be masked by objects in the front. Based on this model, we can isolate the range bin of the metasurface from the surrounding objects [54].

$$S_r = \frac{c_0}{2 * BW}, \quad S = \frac{\#ADC * S_r}{2} \tag{11}$$

where S_r is the range resolution based on BW the bandwidth of the radar, c_0 is the speed of light in free space, S is the

maximum range of the radar, and #*ADC* is the number of ADC samples per chirp. To super-sample a given range bin, a higher number of FFT size than #*ADC* can be used, which enables sub-range-bin thickness of MetaBioLiq metasurface.

6.2 Sweat Signal Extraction

Once we have the clean metasurface reflection signal, we extract the sweat layer reflection in frequency domain $\Gamma_{in}(\omega)$ using the following model [28, 31]:

$$\Gamma_{in}(\omega) = \sum_{n=0}^{\inf} a_n e^{-2n\omega C_1} e^{-j(2n\omega C_2)} \tag{12}$$

compared with the FMCW RX chirp, the extra $e^{-2n\omega C_1}$ and $\omega\tau$ terms represent the attenuation and phase delay from interacting with the material. One major difference between extracted sweat signal vs. RX signal after mixing is the A_0^2 term, which can be modeled as if there is an perfect echo from the top of the metasurface.

6.3 Calibration

In order to extract the sweat S11 as previously modeled, we must calibrate the offset terms from the ADC samples. From [28], the sweat layer's modulation Γ_m based on multiple reflections within the metasurface structure can be isolated as the following:

$$\begin{aligned} \Gamma_m &= S_{11} + \frac{S_{12}S_{21}\Gamma_{in}}{1 - S_{22}\Gamma_{in}}; S_{11} = \Gamma_{m-match} \\ \Gamma_{m-short} &= S_{11} - \frac{S_{12}S_{21}}{1 + S_{22}} = \Gamma_{m-match} - \frac{S_{12}S_{21}}{1 + S_{22}} \end{aligned} \tag{13}$$

where the match (no reflection) and short(total reflection) terms can be measured [31] or synthesized knowing the radar chirp parameters.

In a real mobile application, the match and short terms are extremely challenging to obtain. One cannot assume there is only reflection from the metasurface and the sweat, or measure the maximum reflection at certain position. Thus, we design the adaptive min-max calibration scheme where the min replaces match, and max replaces the short. Based on Eq. (10), we can simulate spectral reflection with metasurface at given range bin as the following:

$$R(\tau_d) = A_0 e^{-2\omega C_1} e^{-j(2n\omega C_2 + \omega\tau_d)} \tag{14}$$

where $R(\tau_d)$ is the synthesized signal, and without reflection can be substituted with additive white Gaussian noise model. Following calibration procedure in [28], the sweat pattern can be modeled as:

$$\Gamma_m = \frac{R(\hat{\tau}) - R(AWGN)}{R(\hat{\tau_d})} \tag{15}$$

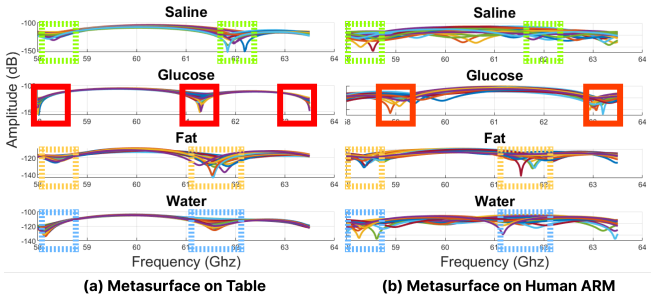

(a) Metasurface on Table (b) Metasurface on Human ARM

Figure 11: Difference categories of sweat content compared with pure water reflection under MetaBioLiq metasurface on (a) table top, (b) human arm. Although some outliners exist, we can observe that general ROI frequency range for saline, fat, and water is consistent.

7 SWEAT SIGNAL COMPREHENSION

7.1 Soft Calibration

Each time the user wears the metasurface, there can be offsets introduced by the mounting process due to the non-rigid surface of the human skin. To remove such offset, we present a soft calibration mechanism that aligns new sensor's reading to baseline. In comparison of Figs. 11 (a) and (b), the saline, fat, and water pattern under the region of interest (ROI) is persistent, while glucose solution's peak frequency ROI drifted by about 1 GHz. Recalling back to Sec. 6.3, the short calibration will use radar reflection without liquid (i.e., air). The Min-Max calibration is performed as the following:

$$\Gamma_{m'}(\omega) = a(\omega) + \left(\frac{(\Gamma_m(\omega) - \min(\Gamma_m(\omega))) \cdot (b(\omega) - a(\omega))}{\max(\Gamma_m(\omega) - \min(\Gamma_m(\omega))} \right) \tag{16}$$

where $a(\omega)$ and $b(\omega)$ are the min and max values across multiple frames in a given frequency ω, respectively. This technique allows a single calibration to counter the placement offset caused signal drift.

7.2 Continuous Sweating

7.2.1 Sweat rate. In order to obtain the integral amount of sweat that the user loses, we continuously monitor the amount of sweat liquid present in the cavity. However, the change in the amount of liquid is subtle and appears in specific frequency spots under the S11 reading, as shown in Fig. 12. Thus, we adopt a compact decision tree algorithm [50] to robustly identify sweat filling based on the tiny variation in the S11 spectrum.

7.2.2 Sweat content. Alongside sweat rate, sweat content educates the user with proper amount of nutrient to sustain wellness or athletic performance. To accurately tune

the sensitivity of MetaBioLiq, we start with different content's contribution in sweat liquid's 1% nonwater volume [43]. The salts of adult sweat range from 10 to 90 $\frac{mM}{L}$ [13], roughly translates to 1000 to 5000 ppm. Glucose is almost insignificant in sweat [73], ranging 0.06 to 0.2 $\frac{mM}{L}$, which roughly translates to 11 to 35 ppm. For fat molecules, due to it's tendency to coagulate with non-polar surface [39, 77], we roughly use 1000 ppm as baseline and dilute it in two folds until 125 ppm. Translation fro mM or $\frac{mM}{L}$ to ppm follows Eq. (17).

$$\text{ppm} = \text{mM} \times \text{Molar Mass (g/mol)} \tag{17}$$

Ideally, linear variation in certain substance concentration may lead to linear or polynomial change in reflection amplitude; however, sweat's tiny presence make such modeling very brittle. In another words, tiny vibrations can lead to complete signal distortion. To maintain robustness against small motion, we adopt a non-linear gradient boosting on shallow decision trees algorithm (i.e., CatBoost [19]) that captures even more subtle difference than the liquid level.

8 EXPERIMENTAL SETUP

In this section, we present MetaBioLiq system's evaluation setup that detects the sweat rate and sweat content.

8.1 Metasurface

We first 3D print a 4 layered metasurface following optimization algorithm in Sec. 5. As shown in Fig. 13, the PLA infill factor of each layer from top to bottom is as follows: 1. 0.5083, 2. 0.527, 3. 0.5379, 4. 0.4371. The liquid cavity on the bottom of the metasurface is 2mm thick, with oval cylinder's major and minor axis lengths 24.6 and 4 mm, respectively. The cavity opens along the major axis, the maximum cavity size of 0.67 mL (667 μL). The size of the metasurface is approximately 42mm in corner-to-corner measurement, less than 47mm in a sports watch [2]. The thickness is set to 2.8cm, which is exactly the length of radar range resolution plus a 1mm thin arch to fit skin curve, the thickness can be optimized in the future with range super-sampling as discussed in Sec. 6.1.

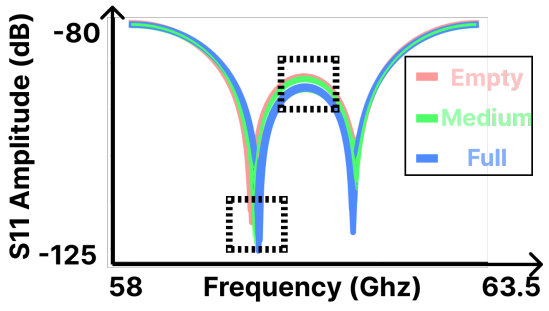

Figure 12: Difference amount of sweat liquid inside the cavity, medium level ranges from 100 μL to 400 μL.

8.2 mmWave Radar

We adopt Infineon's BGT60TR13C 60 GHz FMCW mmWave radar with 5.5 GHz bandwidth [6]. Its ADC sampling rate on the baseband signal is 2.5MHz. To maximize the SINR of the metasurface, we use 512 chirps per frame, with 256 ADC samples per chirp, resulting in about 21.5 MHz ADC sample gap. Given the amount of short time sampling occupying energy and storaging, we limit the slow time frame rate to 5 Hz. Unless otherwise mentioned, the default angle to the person is 0 degree (i.e. head-on), and the default distance is 90 cm. To collect data, we use a Windows 10 laptop with Infineon's Radar Fusion GUI software suite V3.3.0.

8.3 Liquid Preparation

We prepare a total of 24 artificial sweat samples for examination. Including a baseline sample with an empty cavity and a distilled water sample. Generally, human sweat contains 20 to 90 $\frac{mmol}{L}$ of electrolyte [13], which translates to ~ 1000 to ~ 5000 ppm. We prepared 5 saline solutions of 1-5 g per liter of table salt in a 1 g interval, corresponding to 1000 to 5000 ppm sweat electrolyte content. The concentration of glucose in sweat ranges from 0.06 to 0.2 mM that corresponds to 3.3 to 17.3 mM in blood glucose [73]. We prepare 4 glucose solutions from diluting 0.25 g per mL glucose shot drink [8] to 0.03 g per L, then further diluting with distilled water in a 1:1, 1:2, and 1: 3 ratio, matching the sweat glucose levels.

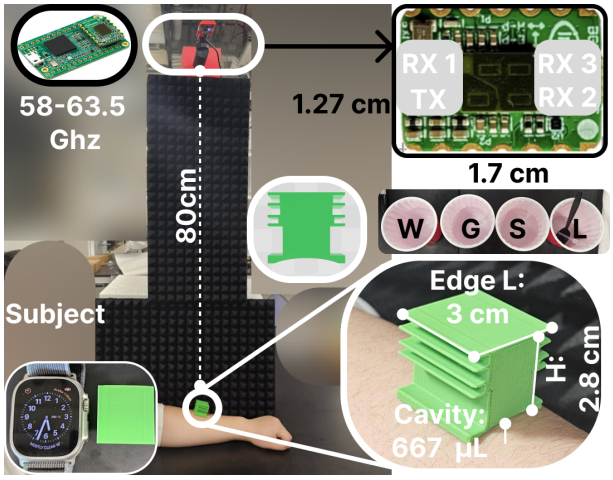

Figure 13: Artificial sweat liquid measurement setup. Three cups of high concentration liquid is prepared, mixed with distilled water to reach different human sweat concentration of liquid.
S-salt, G-glucose, L-lard, W-water.

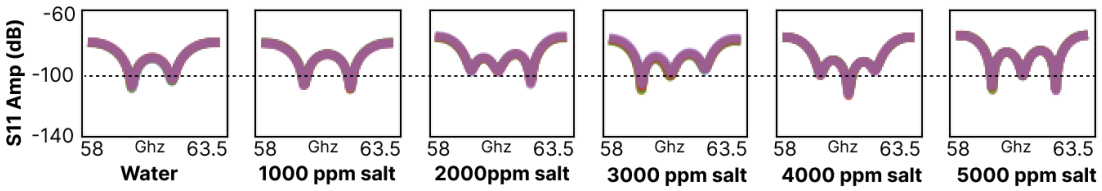

Figure 14: Salt concentration from 2000 to 5000 ppm vs. water.

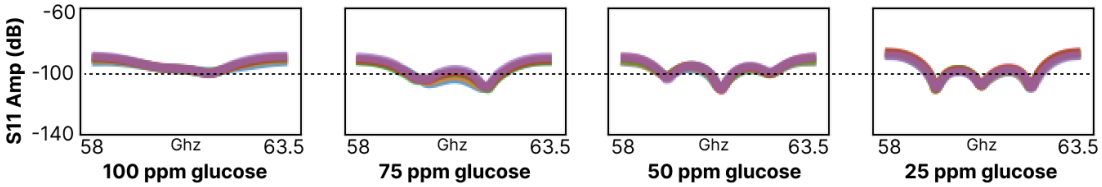

Figure 15: Glucose concentration from 100 to 25 ppm.

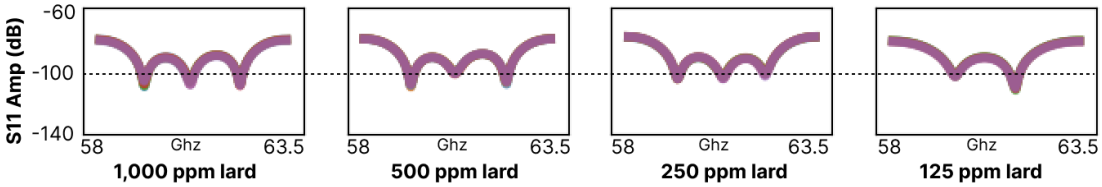

Figure 16: Lard concentration from 1000 to 250 ppm.

Unlike water-soluble electrolyte and glucose, lipids tend to coagulate on the skin surface [39, 62], which is not homogeneous and leads to an ad-hoc concentration. We prepared 4 samples of the lipid mixture by diluting 1g lard grease [4] in 10mL warm water and mixing with distilled water in a 1:1, 1:2 and 1:3 ratio. Furthermore, we mix the above solutions at their highest concentration to form mixtures that better approach the sweat content. This includes salt and glucose mixture at the ratio of 1:1, 1:2, and 2:1, and salt, glucose, lipid mixture at, 1:1:1, 2:1:1, 2:2:1, 1:2:1, 1:2:2, and 1:1:2. A simplified version of differences in S11 vs. concentration is shown in Fig. 14, Fig. 15, and Fig. 16.

8.4 Human Subject

As shown in Fig. 13, we place human arm on top of the table as in writing or typing scenario. The metasurface is placed on top of the human skin with clear tape to fix on the skin. The tape can later be replaced with low-cost skin adhesive use in COTS wearable sensors [48]. All experiments are performed on human subjects, while the microbenchmarks on Sec. 9.3 is performed on a table. A total of 15 subjects, aged 23 to 28, and skin tone ranges from light, brown to dark in 5:5:5 ratio. Most participants also have skin hair on wrist region (10 out of 15). It should be noted that although it is suggested that the participant remain as still as possible, there are subconscious movements and speech-induced vibration and muscle contractions in the range ± 2 cm. To maximize user privacy, we store our user data completely locally, and our study is approved by IRB.

8.5 Model Implementation

We set up two models that both utilize a simple yet robust decision tree structure. First, for liquid level sensing, subtle but deterministic change is classified into 4 classes. Compared to Fig. 12, we divide the medium level from 100-200 μL and 200-400μL for a finer-grained analysis. Each data sample is 1 seconds long, collected at a 5 frame per second radar frame rate, and fixed at 60cm distance. We set the maximum depth of the decision tree to 2 and feed only 30% of 1560 sweat level samples as trainset, and the remaining 70 % data as testset.

For artificial sweat classification, we set the CatBoostClassifer's maximum depth to 6, such that the total number of leaves would not exceed the dimension of our radar input (i.e., 256). The learning rate was set to 1, and loss function is set to Multiclass, as described in Eq. (18):

$$loss = \frac{\sum_{i=1}^{N} w_i \log\left(\frac{e^{a_{it_i}}}{\sum_{j=0}^{M-1} e^{a_{ij}}}\right)}{\sum_{i=1}^{N} w_i} \tag{18}$$

where w_i is the weight, M is the total number of classes, N is the number of samples, a is the logits, and t is the index of ground truth label. We train the model with 25,500 samples and test the model with another 25,500 samples, averaging 1020 samples for every class. Each sample is 5 seconds long, which is equivalent to 25 frames per sample with an array of (25,256). The model was trained for 300 epochs before achieving 96.4% prediction accuracy on the test set, as shown in Fig. 17.

9 EVALUATION

9.1 Metrics

Radar range bin amplitude: The metasurface acts as a passive tag attached on the human body and must be detected by the FMCW radar in its own range bin to clearly extract sweat information. We compare the radar's RX side per range bin amplitude gain from with and without the metasurface to show the RCS σ improvement that the metasurface brings to the sweat liquid.

$$\sigma = \frac{P_r G_t \lambda^2}{P_t G_r (4\pi)^3 R^4} \tag{19}$$

where P_r is the power received by the radar, P_t is the power transmitted by the radar, G_t is the gain of the transmitting antenna, G_r is the gain of the receiving antenna, λ is the wavelength of the radar signal, R is the distance from the radar to the target object.

Classification Accuracy: To characterize MetaBioLiq's liquid identification with tiny change, we use multi-class classification accuracy as follows:

$$Accu = \sum_{i=1}^{M} \frac{(Y_{pred} == Y_{label})}{count(Y_{label})} * 100\% \tag{20}$$

where Y_{label} is the fine-grained label for every sample in Sec. 8.3, M represent 24 classes of sweat liquids. Y_{pred} is the list of all samples predicted by our model.

9.2 Accuracy of Fluid Analysis

9.2.1 Classification of Different Liquid. In order to give feedback on user's nutrient loss during sweating, its essential to characterize the sweat liquid's subtle different in electrolyte, glucose, and lipid mixtures. We present a 24-class model that includes average electrolyte, glucose, and lipid concentrations, as well as complex mixtures. As shown in Fig. 18, the 24 classes of liquid response can be generalized to 10 participants with different skin conditions, different age (25 ± 5) and small movements. In general, the compact model

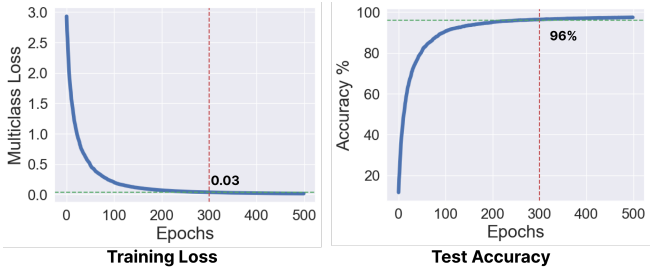

Figure 17: MetaBioLiq's CatBoost model training loss and test accuracy per epoch. To prevent overfitting, the cutoff is at 300 epochs.

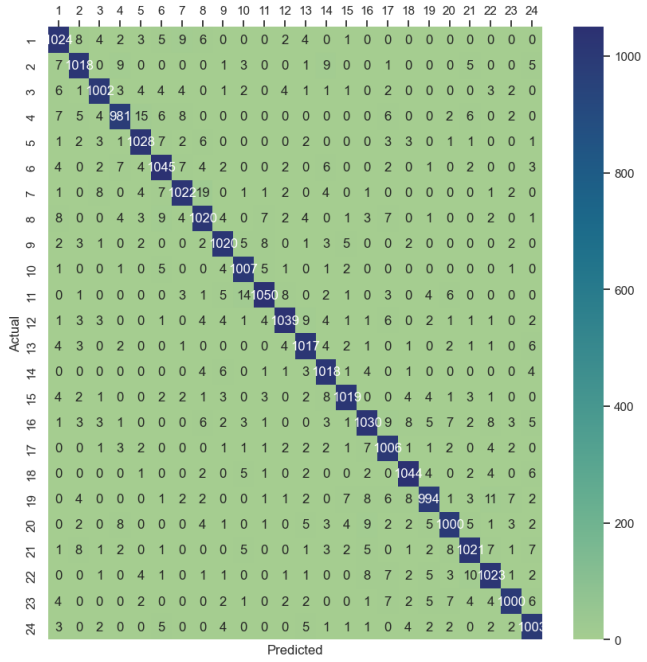

Figure 18: Multiclass confusion matrix from CatBoost classification, darker color symbolizes higher accuracy. The errors are evenly distributed.

Classes	Precision	Accuracy
3	250 μL	100 %
4	125 μL	95 %
6	60 μL	65 %
8	20 μL	33 %

Table 2: Precision vs. Accuracy trade-off.

of MetaBioLiq achieves a 94% accuracy in classifying more than 20,000 sweat signal samples in 24 different artificial sweat liquid mixtures. For example, Fig. 14, Fig. 15, and Fig. 16 show S11 differences from the change in concentration in each category of substance.

9.2.2 Classification of Liquid Level. To continuously record and integrate sweat level, accurate sweat level sensing is crucial. MetaBioLiq achieves 95% accuracy with 4 classes when the user wears the metasurface on the forearm. In a more fine grained experiment, where we attempted to separate sweat volume level up to 8 classes, the performance suffered, as shown in Table 2.

9.3 Micro Benchmarks

We now present a detailed evaluation on various aspects of metasurface design and system configuration.

9.3.1 Different Sized Metasurface. We compare metasurfaces with different edge lengths, while maintaining the same

height and design. We tested the following edge lengths: 1cm, 2cm, 3cm, and 4cm, and found that upon 3 cm edge length, its reflection strength can be significantly distinguished from the surrounding at 60 cm distance. As shown in Fig. 19, 3cm and 4cm lengthed metasurfaces show sufficient RCS and SNR with its own distinguishable range bin.

9.3.2 Different Printer and Filament. To assess different 3D filament or 3D printer's impact on MetaBioLiq metasurface's sensing capability, we examine 4 different colors (R - Bambu Lab, G - Prusa, B - Bambu Lab, W - Bambu Lab). As shown in Fig. 20(a), four colored metasurfaces show synchronized response when measuring the offset that water brings to the metasurface. Although there might be inperfections in the 3D printing process, MetaBioLiq metasurface uses 100% layer infill and PLA material that is easy to handle, lowering the barrier for metasurface design.

9.3.3 Different Radar Parameters. Different radar parameters can satisfy different IoT application with focus on energy consumption, sensing resolution, or sensing rate. On the basis of these three parameters, we tune radar's frame rate, sample per chirp, and chirp per frame to find various optimums. As shown in Table 3, we stress test the frame rate to 2 Hz, ADC samples per chirp to 64, which is roughly 86Mhz per bin resolution, and chirps per frame to 8. Frame rate from 5 Hz to 2 Hz will Overall, the parameter that we chose, focusing on maximizing the SINR from metasurface reflection with 512 chirps per frame, has the highest accuracy.

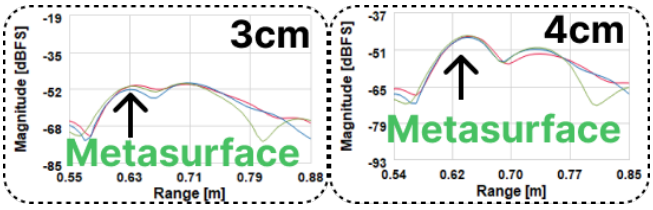

Figure 19: 3 cm edge length is the first size to show distinguishable and comparable reflection strength compared with table background range bin.

Frame Rate	ADC Samples	Chirps/Frame	Accuracy
5	256	512	96 %
2	256	512	96 %
5	64	512	95 %
5	256	8	86 %
2	256	8	51 %
5	16	8	81 %

Table 3: Radar parameter and their corresponding accuracy with exact same model parameters.

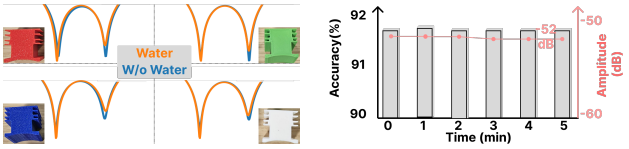

(a) Different colored filament doesn't show significant difference in sensing delta when water is placed under the metasurface.

(b) Overall, temperature change on skin shows insignificant performance change.

Figure 20: Filament color and longitudinal analysis.

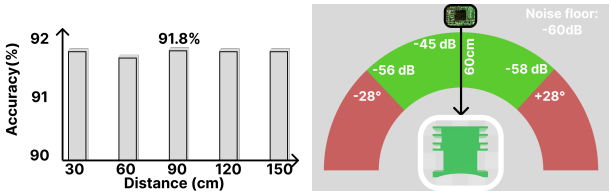

(a) Distance evaluation from 30 cm to 150cm, beyond that, 3cm sized metasurface doesn't show enough range bin SNR.

(b) Both elevation angle and azimuth angle follow the same pattern, given the top spacer is symmetrical.

Figure 21: Distance and angle analysis.

9.4 Robustness in Real-World Settings

9.4.1 Temperature Impedance Shift. To quantify and verify the temperature induced impedance shift [9] in microliter level, we apply 667 μL of room temperature solution 25$^{\circ}C$ on participant's forearm skin, and record 5 minutes of continuous data to identify the drift to 30$^{\circ}C \pm 2^{\circ}C$. As shown in Fig. 20(b), both the accuracy and the amplitude of the radar range bin signal did not change significantly. This proves that our modeling on different material' dielectric constant at room temperature suffices in the low activity use case.

9.4.2 Distance. We proceed to evaluate the performance with respect to different distances and practical setup considerations. As shown in Fig. 21(a), up to 1.5 meters away, the signal from the metasurface is still distinguishable from the arm, where as beyond that, it becomes challenging to align and measure the sweat signal. Generally speaking, if the size of the metasurface increases from 3cm, the sensing range could be further increased due to RCS gain, but at the cost of practicality. As shown in Fig. 13, with MetaBioLiq metasurface size showing sufficient RSC/SINR, and still compact in size, with diagonal length smaller than a COTS smart watch.

9.4.3 Angle. Even in relatively static scenarios, human body will naturally breathe, twitch, and unconsciously move their arm as well as other parts of the body [36]. We explore the boundary that the current flat-headed metasurface can still reflect sufficient energy to deliver sweat information. As

shown in Fig. 21(b), the fast headed metasurface is capable of being identified from ±28 degree azimuth and elevation angles from the top view. Beyond this range, the radar signal either does not reach the bottom layer of the metasurface or is reflected specularly to another direction.

10 DISCUSSION AND LIMITATIONS

Radar vs. VNA: Although our mmWave radar calibration turns a mmWave radar into a pseudo-VNA probe, its frequency domain resolution is limited to the number of ADC samples. With the same radar [6], it can reach a maximum of 2048 ADC samples per chirp, 1000 frames per second, or 512 chirps per frame. The trade-off is between the frame duration, number of chirps per frame, and number of ADC samples per chirp. In this paper, we sacrificed frequency domain resolution and used 256 ADC samples to sweep the 5.5 GHz bandwidth, resulting in $\sim 20MHz$ frequency resolution.
Other RF bands: Generally speaking, higher RF frequency with lower wavelength is more sensitive to smaller objects (i.e., thinner layer of liquid) [55]. With help from metasurfaces that match impedance and resonate with material in contact, other frequencies (e.g., 5 GHz Wi-Fi with 6 cm wavelength, 24 GHz mmWave with ~ 1.25 cm wavelength, 150 GHz with 2mm wavelength) can also enable a wide range of applications with the same design.
Glucose Sensitivity: Although sweat glucose level and blood glucose level is highly correlated [73], its concentration in sweat is relatively low, and has less impact to sweat dielectric than electrolyte, making it more challenging to sense accurately.
Motion Impact: The fundamental metasurface design lacks rigorous exercise motion support such as running or basketball. Although techniques like micro-Doppler [16] can expliot side lobe information, its bottleneck is still on RCS and SNR. To make a motion-resilent system, one can explore metal-based metasurface design, as well as combinations of reflection lens such as the Van Atta array used in [49]. Compared with active systems, which the tag does both sensing and communication, passive systems rely on relatively stationary radar to tag position. However, this is a common limitation in passive sensing systems that needs to be addressed.
User Experience: We used PLA material for our metasurface that costs less than $1 each with 3cm of edge length. There are many 3D print materials that are skin friendly (e.g., thermoplastic polyurethane that is soft or special PLA that is food grade [38]) that has a slight change in the dielectric parameter compared to the PLA material of MetaBioLiq.
Future Applications: MetaBioLiq metasurface has many advantages. It is easy to model, low cost to fabricate, versatile with different material, and can be made into various form-factors (large or small). An attractive application is in-body biofluid characterization that assists current camera-only capsule endoscopy. With mmWave radar antenna in the scale of millimeters, and a small liquid cavity in close range, food grade material made metasurface can open new paths in in-vivo sensing. In addition, given mmWave radar's beamforming capability, a single multi-antenna mmWave radar can support multi-user scenarios such as in a gym.

11 CONCLUSION

In this work, we present a passively remote, wearable, and 3D-printable metasurface that allows biofluid detection at the microliter level. MetaBioLiq allows sweat liquid content to be identified remotely without any electrical circuit on the human skin. Instead, it's 3D printed PLA metasurface can be easily manufactured, sensed at 1.5 m, and able to tell various concentrations of electrolyte, glucose, and lipid in 500 microliters of sweat fluid. Extensive experiments have shown that MetaBioLiq can correctly identify sweat content on 10 different people's skin with over 96% accuracy, with only microliters of sweat traped in a passive cavity. In addition, we explore different possibilities of the sensing system to assist future explorations in nonintrusive biomedical or even in vivo applications. In conclusion, MetaBioLiq has the potential to serve the future medical world with its accessibility, accuracy, and flexibility.

ACKNOWLEDGEMENT

We wholeheartedly thank our shepherd and all anonymous reviewers for their insightful comments and feedback. The work reported in this paper is supported in part by the NSF under Grants CNS-1901048, CNS-1925767, CNS-2128588, CNS-2312715, and CNS-2408393.

REFERENCES

[1] 2017. Skin to e-skin. Nature Nanotechnology 12 (2017), 1017. https://doi.org/10.1038/nnano.2017.228 Accessed: 2024-03-12.
[2] 2024. Apple Watch Ultra. https://www.apple.com/shop/buy-watch/apple-watch-ultra. Accessed: 03-15-2024.
[3] 2024. E8361A PNA Network Analyzer, 10 MHz to 67 GHz [Obsolete]. https://www.keysight.com/us/en/product/E8361A/pna-series.html. Accessed: 2024-03-09.
[4] 2024. Farmer John Lard 4lb. https://www.walmart.com/ip/Farmer-John-Lard-4lb/2499123321. Accessed: 2024-03-12.
[5] 2024. Research and Development. https://nixbiosensors.com/pages/research-and-development. Accessed: 2024-03-09.
[6] Infineon Technologies AG. 2024. BGT60TR13C XENSIV™ 60GHz radar sensor for advanced sensing. https://www.infineon.com/cms/en/product/sensor/radar-sensors/radar-sensors-for-iot/60ghz-radar/bgt60tr13c/. Accessed: 2024-03-11.
[7] SI Alekseev, AA Radzievsky, MK Logani, and MC Ziskin. 2008. Millimeter wave dosimetry of human skin. Bioelectromagnetics: Journal of the Bioelectromagnetics Society, The Society for Physical Regulation

in Biology and Medicine, The European Bioelectromagnetics Association 29, 1 (2008), 65–70.

[8] American Diabetes Association. 2024. ReliOn Glucose Shot. https://consumerguide.diabetes.org/products/relion-glucose-shot. Accessed: 2024-03-12.

[9] Andrei Andryieuski, Svetlana M Kuznetsova, Sergei V Zhukovsky, Yuri S Kivshar, and Andrei V Lavrinenko. 2015. Water: Promising opportunities for tunable all-dielectric electromagnetic metamaterials. Scientific reports 5, 1 (2015), 1–9.

[10] Lindsay B Baker. 2019. Physiology of sweat gland function: The roles of sweating and sweat composition in human health. Temperature 6, 3 (2019), 211–259.

[11] Mallika Bariya, Hnin Yin Yin Nyein, and Ali Javey. 2018. Wearable sweat sensors. Nature Electronics 1, 3 (2018), 160–171.

[12] JMG Barthel and Richard Buchner. 1991. High frequency permittivity and its use in the investigation of solution properties. Pure and Applied Chemistry 63, 10 (1991), 1473–1482.

[13] Graham P Bates and Veronica S Miller. 2008. Sweat rate and sodium loss during work in the heat. Journal of Occupational Medicine and Toxicology 3 (2008), 1–6.

[14] Arnold E. Bender and David A. Bender. 1995. Surface Area of Human Skin. https://bionumbers.hms.harvard.edu/bionumber.aspx?s=y&id=100578&ver=1. Accessed: 2024-03-09.

[15] Adam R Carr, Yash H Patel, Charles R Neff, Sadaf Charkhabi, Nathaniel E Kallmyer, Hector F Angus, and Nigel F Reuel. 2020. Sweat monitoring beneath garments using passive, wireless resonant sensors interfaced with laser-ablated microfluidics. NPJ digital medicine 3, 1 (2020), 62.

[16] Victor C Chen, Fayin Li, S-S Ho, and Harry Wechsler. 2006. Micro-Doppler effect in radar: phenomenon, model, and simulation study. IEEE Transactions on Aerospace and electronic systems 42, 1 (2006), 2–21.

[17] Romit Roy Choudhury. 2021. Earable computing: A new area to think about. In International Workshop on Mobile Computing Systems and Applications. 147–153.

[18] Ashutosh Dhekne, Mahanth Gowda, Yixuan Zhao, Haitham Hassanieh, and Romit Roy Choudhury. 2018. Liquid: A wireless liquid identifier. In Proceedings of ACM MobiSys.

[19] Anna Veronika Dorogush, Vasily Ershov, and Andrey Gulin. 2018. CatBoost: gradient boosting with categorical features support. arXiv preprint arXiv:1810.11363 (2018).

[20] Stephen Eichhorn, JWS Hearle, M Jaffe, and T Kikutani. 2009. Handbook of textile fibre structure: Volume 1: fundamentals and manufactured polymer fibres. (2009).

[21] Angie R Eldamak, Sarah Thorson, and Elise C Fear. 2020. Study of the dielectric properties of artificial sweat mixtures at microwave frequencies. Biosensors 10, 6 (2020), 62.

[22] Chao Feng, Jie Xiong, Liqiong Chang, Ju Wang, Xiaojiang Chen, Dingyi Fang, and Zhanyong Tang. 2019. WiMi: Target material identification with commodity Wi-Fi devices. In IEEE International Conference on Distributed Computing Systems (ICDCS).

[23] DH Gadani, VA Rana, SP Bhatnagar, AN Prajapati, and AD Vyas. 2012. Effect of salinity on the dielectric properties of water. (2012).

[24] Fupeng Gao, Chunxiu Liu, Lichao Zhang, Tiezhu Liu, Zheng Wang, Zixuan Song, Haoyuan Cai, Zhen Fang, Jiamin Chen, Junbo Wang, et al. 2023. Wearable and flexible electrochemical sensors for sweat analysis: a review. Microsystems & Nanoengineering 9, 1 (2023), 1–21.

[25] Carl V. Gisolfi. 1993. Water Requirements During Exercise in the Heat. https://www.ncbi.nlm.nih.gov/books/NBK236237/. Accessed: 2024-03-09.

[26] Jian Gong, Xinyu Zhang, Kaixin Lin, Ju Ren, Yaoxue Zhang, and Wenxun Qiu. 2021. RF vital sign sensing under free body movement. Proceedings of the ACM on Interactive, Mobile, Wearable and Ubiquitous Technologies 5, 3 (2021).

[27] Sijia Gu, Tianjun Lin, and Tuami Lasri. 2016. Broadband dielectric characterization of aqueous saline solutions by an interferometer-based microwave microscope. Applied Physics Letters 108, 24 (2016).

[28] Ahmed Metwally Hegazy. 2021. Remote material characterization using mmWave FMCW radar with complex baseband. Master's thesis. University of Waterloo.

[29] Yongzhi Huang, Kaixin Chen, Yandao Huang, Lu Wang, and Kaishun Wu. 2021. Vi-liquid: unknown liquid identification with your smartphone vibration. In Proceedings of ACM MobiCom.

[30] Kaisarul Islam, Tabia Hossain, Mohammad Monirujjaman Khan, Mehedi Masud, and Roobaea Alroobaea. 2021. Comparative Design and Study of A 60 GHz Antenna for Body-Centric Wireless Communications. Computer Systems Science & Engineering 37, 1 (2021).

[31] Timo Jaeschke, Simon Kueppers, Nils Pohl, and Jan Barowski. 2022. Calibrated and frequency traceable D-band FMCW radar for VNA-like S-parameter measurements. In IEEE Radio and Wireless Symposium (RWS). IEEE, 64–67.

[32] Wenli Jiao, Yanlin Li, Xiangdong Xi, Ju Wang, Dingyi Fang, and Xiaojiang Chen. 2023. BioScatter: Low-Power Sweat Sensing with Backscatter. In Proceedings of the 21st Annual International Conference on Mobile Systems, Applications and Services. 191–204.

[33] ZHOU Juan, MEN Dong, and Xian-En Zhang. 2022. Progress in wearable sweat sensors and their applications. Chinese Journal of Analytical Chemistry 50, 2 (2022), 87–96.

[34] Ashish Kalkal, Sumit Kumar, Pramod Kumar, Rangadhar Pradhan, Magnus Willander, Gopinath Packirisamy, Saurabh Kumar, and Bansi Dhar Malhotra. 2021. Recent advances in 3D printing technologies for wearable (bio) sensors. Additive Manufacturing 46 (2021), 102088.

[35] Tutku Karacolak, Elaine C Moreland, and Erdem Topsakal. 2013. Cole–cole model for glucose-dependent dielectric properties of blood plasma for continuous glucose monitoring. Microwave and Optical Technology Letters 55, 5 (2013), 1160–1164.

[36] Andrei Khrennikov. 1998. Human subconscious as ap-adic dynamical system. Journal of Theoretical Biology 193, 2 (1998), 179–196.

[37] Taeil Kim, Qian Yi, Emily Hoang, and Rahim Esfandyarpour. 2021. A 3D printed wearable bioelectronic patch for multi-sensing and in situ sweat electrolyte monitoring. Advanced Materials Technologies 6, 4 (2021), 2001021.

[38] Jakub Kočí. 2020. How to make food-grade 3D printed models. https://blog.prusa3d.com/how-to-make-food-grade-3d-printed-models_40666/. Accessed: 2024-03-12.

[39] Wayne W. LaMorte. 2016. Lipids - Basic Cell Biology. https://sphweb.bumc.bu.edu/otlt/mph-modules/ph/ph709_basiccellbiology/PH709_BasicCellBIology4.html. Accessed: 2024-03-11.

[40] Yumeng Liang, Anfu Zhou, Huanhuan Zhang, Xinzhe Wen, and Huadong Ma. 2021. Fg-liquid: A contact-less fine-grained liquid identifier by pushing the limits of millimeter-wave sensing. Proceedings of the ACM on Interactive, Mobile, Wearable and Ubiquitous Technologies 5, 3 (2021), 1–27.

[41] Tianjun Lin, Sijia Gu, and Tuami Lasri. 2017. Highly sensitive characterization of glucose aqueous solution with low concentration: Application to broadband dielectric spectroscopy. Sensors and Actuators A: Physical 267 (2017), 318–326.

[42] Absolute Markets. 2019. Global Sweat Sensors Market is Expected to Reach USD 2,591.19 Million by 2027 - Growing at a CAGR of 9.6% Owing to Rising Investment of Market Participants for Development of Technologically Advanced Products, Says Absolute Markets. https:

//tinyurl.com/y7kpchxh. Accessed: 2024-02-29.
[43] MedlinePlus. 2023. Sweating - Health Video. https://medlineplus.gov/ency/anatomyvideos/000127.htm. Accessed: 2024-03-09.
[44] Thomas Meissner and Frank J Wentz. 2004. The complex dielectric constant of pure and sea water from microwave satellite observations. IEEE Transactions on Geoscience and remote Sensing 42, 9 (2004), 1836–1849.
[45] Scanning Probe Microscopy. 2007. Scanning probe microscopy.
[46] Scott J Montain and Edward F Coyle. 1992. Influence of graded dehydration on hyperthermia and cardiovascular drift during exercise. Journal of applied physiology 73, 4 (1992), 1340–1350.
[47] James Moyer, Donald Wilson, Irina Finkelshtein, Bruce Wong, and Russell Potts. 2012. Correlation between sweat glucose and blood glucose in subjects with diabetes. Diabetes technology & therapeutics 14, 5 (2012), 398–402.
[48] Nix Biosensors. 2023. Hydration Biosensor. https://nixbiosensors.com/collections/all-products/products/hydration-biosensor. Accessed: 2023-03-10.
[49] John Nolan, Kun Qian, and Xinyu Zhang. 2021. RoS: passive smart surface for roadside-to-vehicle communication. In ACM SIGCOMM.
[50] F. Pedregosa, G. Varoquaux, A. Gramfort, V. Michel, B. Thirion, O. Grisel, M. Blondel, P. Prettenhofer, R. Weiss, V. Dubourg, J. Vanderplas, A. Passos, D. Cournapeau, M. Brucher, M. Perrot, and E. Duchesnay. 2011. Scikit-learn: Machine Learning in Python. Journal of Machine Learning Research 12 (2011), 2825–2830.
[51] Kun Qian, Lulu Yao, Xinyu Zhang, and Tse Nga Ng. 2022. MilliMirror: 3D printed reflecting surface for millimeter-wave coverage expansion. In Proceedings of ACM MobiCom.
[52] Amin Ranjbar and Anthony Grbic. 2017. Analysis and synthesis of cascaded metasurfaces using wave matrices. Phys. Rev. B 95 (May 2017), 205114. Issue 20. https://doi.org/10.1103/PhysRevB.95.205114
[53] Amin Ranjbar and Anthony Grbic. 2019. Broadband, Multiband, and Multifunctional All-Dielectric Metasurfaces. Phys. Rev. Appl. 11 (May 2019), 054066. Issue 5. https://doi.org/10.1103/PhysRevApplied.11.054066
[54] Mark A Richards, Jim Scheer, William A Holm, and William L Melvin. 2010. Principles of modern radar. (2010).
[55] Edward J Rothwell and Michael J Cloud. 2018. Electromagnetics. CRC press.
[56] Yiwei Ru, Peipei Li, Muyi Sun, Yunlong Wang, Kunbo Zhang, Qi Li, Zhaofeng He, and Zhenan Sun. 2023. Sensing Micro-Motion Human Patterns using Multimodal mmRadar and Video Signal for Affective and Psychological Intelligence. In Proceedings of the 31st ACM International Conference on Multimedia. 5935–5946.
[57] Fei Shang, Panlong Yang, Yubo Yan, and Xiang-Yang Li. 2022. LiqRay: non-invasive and fine-grained liquid recognition system. In Proceedings of ACM MobiCom.
[58] Mohamed Sharafeldin, Abby Jones, and James F Rusling. 2018. 3D-printed biosensor arrays for medical diagnostics. Micromachines 9, 8 (2018), 394.
[59] Vitali Sikirzhytski, Aliaksandra Sikirzhytskaya, and Igor K Lednev. 2012. Multidimensional Raman spectroscopic signature of sweat and its potential application to forensic body fluid identification. (2012).
[60] Jinhie Skarda, Rahul Trivedi, Logan Su, Diego Ahmad-Stein, Hyounghan Kwon, Seunghoon Han, Shanhui Fan, and Jelena Vučković. 2022. Simulation of large-area metasurfaces with a distributed transition matrix method. Conference on Lasers and Electro-Optics (2022). https://doi.org/10.1364/cleo_qels.2022.fm5h.6
[61] Xue Sun, Wenwen Deng, Xudong Wei, Dingyi Fang, Baochun Li, and Xiaojiang Chen. 2023. Akte-liquid: Acoustic-based liquid identification with smartphones. ACM Transactions on Sensor Networks 19, 1 (2023).
[62] T Takemura, PW Wertz, and K Sato. 1989. Free fatty acids and sterols in human eccrine sweat. British Journal of Dermatology 120, 1 (1989), 43–47.
[63] Marco Vari and Dajana Cassioli. 2014. mmWaves RSSI indoor network localization. In 2014 IEEE International Conference on Communications Workshops (ICC). IEEE, 127–132.
[64] Vessel Health. 2023. Vessel Health Wellness Urine Test, at-Home Urine Test Kit to Measure Hydration, pH, Ketones, and More, Essential 8 Test Strips - 7 Pack. https://www.amazon.com/Vessel-Health-Wellness-Urine-Test/dp/B0CQ5HL9KM. Accessed: 2023-03-10.
[65] Hao Wang, Daqing Zhang, Yasha Wang, Junyi Ma, Yuxiang Wang, and Shengjie Li. 2016. RT-Fall: A real-time and contactless fall detection system with commodity WiFi devices. IEEE Transactions on Mobile Computing 16, 2 (2016), 511–526.
[66] Ju Wang, Jie Xiong, Xiaojiang Chen, Hongbo Jiang, Rajesh Krishna Balan, and Dingyi Fang. 2017. TagScan: Simultaneous target imaging and material identification with commodity RFID devices. In Proceedings of ACM MobiCom.
[67] Zhu Wang, Yifan Guo, Zhihui Ren, Wenchao Song, Zhuo Sun, Chao Chen, Bin Guo, and Zhiwen Yu. 2024. LiqDetector: Enabling Container-Independent Liquid Detection with mmWave Signals Based on a Dual-Reflection Model. Proceedings of the ACM on Interactive, Mobile, Wearable and Ubiquitous Technologies 7, 4 (2024), 1–24.
[68] Teng Wei and Xinyu Zhang. 2015. mTrack: High-precision passive tracking using millimeter wave radios. In ACM Annual International Conference on Mobile Computing and Networking.
[69] Chenshu Wu, Feng Zhang, Beibei Wang, and KJ Ray Liu. 2020. mSense: Towards mobile material sensing with a single millimeter-wave radio. Proceedings of the ACM on Interactive, Mobile, Wearable and Ubiquitous Technologies 4, 3 (2020), 1–20.
[70] Ting Wu, Theodore S Rappaport, and Christopher M Collins. 2015. The human body and millimeter-wave wireless communication systems: Interactions and implications. In IEEE International Conference on Communications (ICC). IEEE, 2423–2429.
[71] Yuyong Xiong, Songxu Li, Changzhan Gu, Guang Meng, and Zhike Peng. 2021. Millimeter-wave bat for mapping and quantifying micro-motions in full field of view. Research (2021).
[72] Hongfei Xue, Qiming Cao, Chenglin Miao, Yan Ju, Haochen Hu, Aidong Zhang, and Lu Su. 2023. Towards generalized mmwave-based human pose estimation through signal augmentation. In Proceedings of ACM MobiCom.
[73] Hima Zafar, Asma Channa, Varun Jeoti, and Goran M Stojanović. 2022. Comprehensive review on wearable sweat-glucose sensors for continuous glucose monitoring. Sensors 22, 2 (2022), 638.
[74] Hanbin Zhang, Gabriel Guo, Emery Comstock, Baicheng Chen, Xingyu Chen, Chen Song, Jerry Ajay, Jeanne Langan, Sutanuka Bhattacharjya, Lora A Cavuoto, et al. 2020. RehabPhone: a software-defined tool using 3D printing and smartphones for personalized home-based rehabilitation. In Proceedings of the 18th international conference on mobile systems, applications, and services. 434–447.
[75] Hanbin Zhang, Aosen Wang, Dongmei Li, and Wenyao Xu. 2018. Deepvoice: A voiceprint-based mobile health framework for parkinson's disease identification. In 2018 IEEE EMBS International Conference on Biomedical & Health Informatics (BHI). IEEE, 214–217.
[76] Mingmin Zhao, Fadel Adib, and Dina Katabi. 2016. Emotion recognition using wireless signals. In Proceedings of the 22nd annual international conference on mobile computing and networking. 95–108.
[77] Xinhua Zhu, Wenchuan Guo, Dayang Liu, and Fei Kang. 2018. Determining the fat concentration of fresh raw cow milk using dielectric spectroscopy combined with chemometrics. Food analytical methods 11 (2018), 1528–1537.